applied sciences

MDPI

Article

Wind-Wave-Current Coupled Modeling of the Effect of Artificial Island on the Coastal Environment

Guowei Fu [1,2], Jian Li [2,*], Kun Yuan [1,*], Yanwei Song [1], Miao Fu [1], Hongbing Wang [1] and Xiaoming Wan [1]

[1] Haikou Research Center of Marine Geology, China Geological Survey, Haikou 571127, China; fuguowei@mail.cgs.gov.cn (G.F.); songyanwei@mail.cgs.gov.cn (Y.S.); fumiao@mail.cgs.gov.cn (M.F.); wanghongbing@mail.cgs.gov.cn (H.W.); wanxiaoming@mail.cgs.gov.cn (X.W.)
[2] College of Marine Science and Technology, China University of Geosciences, Wuhan 430074, China
* Correspondence: lijian_cky@hotmail.com (J.L.); yuankun01@mail.cgs.gov.cn (K.Y.)

Abstract: The effect of artificial island on the geomorphologic processes in the coastal area under the coupled hydrodynamics, wave, and sediment transport system is a complicated and multi-scale problem. Studying these dynamic processes will suggest how coastal ecological restoration should be conducted. In this study, a unified, unstructured, gridded coupled hydrodynamics, wave, and sediment transport model and a topographic evolution model were adopted. Based on the field observations of water depth, velocity, suspended sediment concentration, bed sand, and quaternary thickness, a high-spatiotemporal-resolution numerical simulation of the offshore dynamic environment under the disturbance of artificial island was performed, and the accuracy of the calculation was verified. The research showed that the coupling system with an unstructured mesh was able to reproduce the flow and sediment transport processes with acceptable accuracy. The contracted flow zone between the artificial island and the coastline, the runoff and alongshore current from the river, as well as the tidal flow from the ocean, worked together to mold the local complex morphology around the artificial island. The coupled modeling system, supported with parallel computation, can be used to study coastal environments with small-scale wading structures.

Keywords: coastal engineering; artificial island; coupled modeling system; parallel computation

check for updates

Citation: Fu, G.; Li, J.; Yuan, K.; Song, Y.; Fu, M.; Wang, H.; Wan, X. Wind-Wave-Current Coupled Modeling of the Effect of Artificial Island on the Coastal Environment. *Appl. Sci.* **2023**, *13*, 7171. https://doi.org/10.3390/app13127171

Academic Editor: Marta Pérez Arlucea

Received: 26 April 2023
Revised: 9 June 2023
Accepted: 12 June 2023
Published: 15 June 2023

1. Introduction

With the rapid development of society and economies in coastal areas of China, the contradiction between the shortage of land resources and development is becoming more and more prominent. Artificial islands became an effective method for human beings to expand production and living space into the sea and alleviate the human–land contradiction in coastal areas [1]. Hainan is a province seeing the rapid development of artificial island. According to statistics, from 2000 to 2014, Hainan approved the construction of 11 artificial islands, totaling 1845.34 hm^2. However, unreasonable land reclamation also brings about corresponding negative environmental and ecological effects, such as the decline in the quality of the marine environment, habitat degradation, destruction of the ecological balance, changes in the hydrodynamic environment, erosion and siltation of the shoreline, etc., which is particularly significant for sandy coasts and coastal areas [2,3].

Under current national policy and because of the demand for the construct of an ecological civilization and shoal restoration, research on the coastal erosion and siltation caused by artificial island is also being carried out by various scientific and technological workers. The traditional method is to use multi-stage remote sensing interpretation analysis to check the scale of the impact of the artificial island's construction on the adjacent coastline. For example, Yang Yanxiong et al. [4] analyzed the changes in the coastline before and after the construction of an artificial island by using remote sensing image interpretation. Li Songzhe [5] applied a one-dimensional coastal shoreline evolution model based on the principle of the conservation of mass to evaluate the development of changes to the

erosion and siltation of the nearby shoreline before and after the construction of man-made islands. However, using remote sensing image analysis and one-dimensional simulation, it is difficult to understand the dynamic development process of artificial island' impacts on the nearby sea area at high spatial and temporal resolutions.

Most studies on the stability of the shorelines of artificial island were carried out by establishing relevant numerical models and conducting a comprehensive analysis and evaluation of the influence of artificial islands on the stability of the shoreline through the simulation of regional wave, tide, and sediment change characteristics before and after the island's construction. Jetro [6] studied the feasibility of constructing an artificial island at the Pacific entrance of the Panama Canal in 2002. The artificial island was filled using earth excavated for the expansion of the Panama Canal. Bayyinch [7] studied the impact of Palm Tree Island in Dubai on the marine environment in the Persian Gulf in 2006. They analyzed the impact of artificial island construction on marine organisms and marine sediment movement and evaluated the compliance of artificial island construction with local marine environmental protection laws and regulations. In China, Gong Wenping et al. [8] used the DELFT3D model based on a structural grid to discuss the influence of building sun and moon islands under different schemes on the hydrodynamic conditions and sediment transport in coastal areas. However, a structural grid is unable to reflect the complex coastline and local geometric features of artificial islands. Tan and Gao [9] applied the FVCOM model of ocean dynamics based on an unstructured grid to evaluate the influence of the proposed construction of the new Sanya Airport artificial island in Hainan Province on the surrounding hydrodynamics. The results showed that the unstructured grid model can accurately reflect the boundaries of local buildings and is suitable for simulating problems across physical scales, which can significantly improve the simulation accuracy. However, there is a nonlinear response relationship between artificial island and natural driving forces (such as typhoons and waves, etc.). For example, Kuang Cuiping et al. [10] used the MIKE21 model based on an unstructured grid to study the influence of the nonlinear superposition effect on tidal currents and waves when artificial island and coastal remediation projects co-exist. Yang Fan et al. [11] used a mathematical model of typhoon winds and waves to analyze wave elements under extreme weather in the presence of the artificial island of the Hong Kong–Zhuhai–Macao Bridge.

According to previous studies, it is necessary to use an unstructured grid ocean dynamics model when considering the dynamic nonlinear processes of hydrodynamics, waves, sediment transport, and topographic evolution affecting the nearshore area under the coupling of artificial island and natural driving forces. When a complex coupled mathematical model of wind and wave flow is used to study offshore dynamic processes under the disturbance of artificial island, a large number of basic data-driven models are needed to obtain reliable initial and boundary conditions of the model, which was lacking in previous numerical simulation studies on the influence of artificial island on the offshore environment [12,13]. Meanwhile, when mathematical models with different spatial-temporal evolution scales are coupled, such as the hydrodynamic, wave, and sediment transport models mentioned above, couplers are usually used for spatial interpolation [8], and interpolation errors will be introduced no matter what interpolation algorithm is used.

In this study, the marine area around the artificial island of Qionghai City, Hainan Province, was taken as the research object, and a unified unstructured grid marine dynamics SCHISM simulation system [14,15] was adopted to complete the simulation of the wind, wave, current, and sediment transport systems. Combined with a large number of field-measured data including sounding, velocity, suspended sediment, and bed sand and quaternary bed sand thickness in the surrounding marine area collected in 2020 and 2021, a simulation study on the influence of artificial island on the coastal environment under a coupled model of the wind, waves, current [16], and sediment transport [17] was carried out. The proposed approach improved the simulation accuracy of inshore environments across multiple scales (transition from small-scale artificial island to large-scale open ocean boundary).

2. Materials and Methods

2.1. Study Area

The study area was the waters around an artificial island—in, Qionghai City, Hainan Island. The artificial island is the only artificially reclaimed island in Boao Town, Qionghai City, Hainan Province, about 6.8 km north of the mouth of the Wanquan River (Figure 1a). The study area is a tropical monsoon climate, with an average annual temperature of about 25.0 °C and an average annual precipitation of 2103.0 mm. According to the wind data from Qionghai-Wanning Meteorological Station, from 1981 to 2010, the average annual wind speed in Qionghai was 2.2 m/s, and the prevailing wind direction was mainly southerly in summer and northerly in winter. Spring and autumn represent the transition seasons between the two wind directions (Figure 1b). The tides were irregular semi-diurnal tides. The normal wave direction throughout the year was southeast, which was the main wave direction. At the same time, the coast will be affected by the Taiwan wave and the near sea wave; the sub-normal wave direction was SSE; the strong wave direction was ESE, SE, and SSE; and the SE and SSE wave directions account for 68% of the total frequency (Figure 1c).

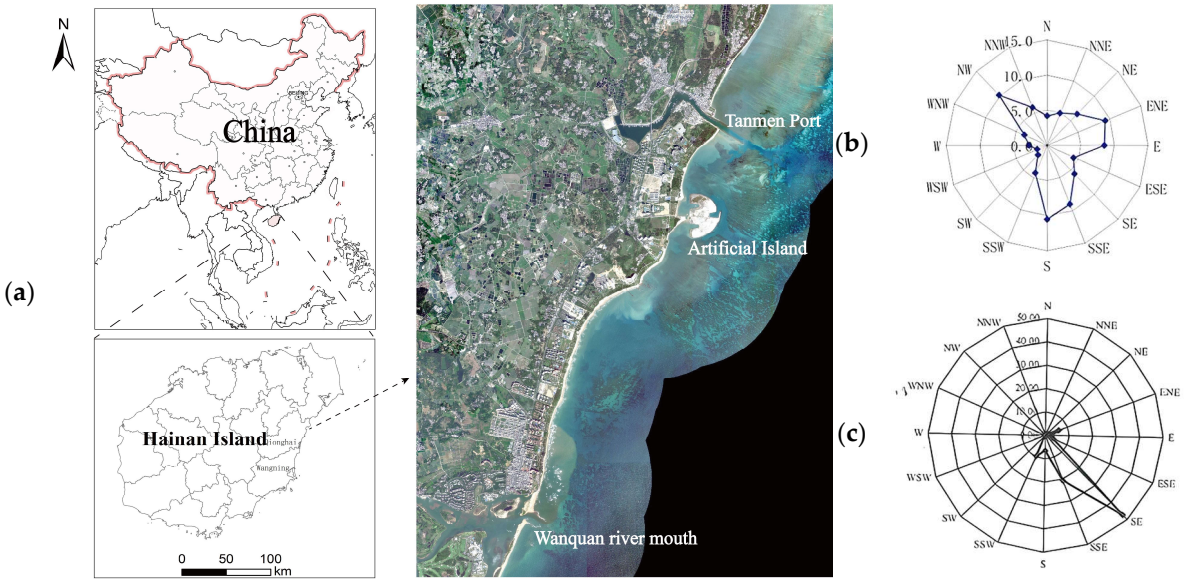

Figure 1. (**a**) Study area. (**b**) Rose chart of annual mean wind power in the study area. (**c**) Annual mean wave rose map of sea area around the study area.

The construction of an artificial island began in 2011, with a circumference of 4040 m and an area of 4.61×10^5 m^2. However, due to environmental problems along the shoreline, construction was stopped, and the shoreline restoration project was launched in 2021. The whole artificial island section presents the phenomenon of siltation in the middle channel and erosion on the north and south sides of the channel. Since the construction of the artificial island in 2011, the phenomenon of erosion and siltation was significantly intensified. The maximum annual average erosion and siltation distance were about 55.6 m/a and 10.2 m/a, respectively, which increased by about 22 times and 5 times compared to before construction. The monitoring data of the bank profile in 2020 showed that erosion and sedimentation occurred in both normal seasonal weather and typhoon weather, and the variation in erosion and sedimentation in the north and south coast sections increased by 2 times and 6 times, respectively, after the passage of typhoons. The reclamation of the artificial island changed the regional hydrodynamics, which were superimposed with the influence of extreme weather such as typhoons. Waves scour the loose shoals of the north and south coasts, which intensified erosion and increased the concentration of coastal suspended sediment. This sediment accumulated in the wave shadow area with weak hydrodynamics on the west side of the artificial island to form

an intermediate silting salient [18]. In addition, the hydrodynamic environment around the artificial island was also affected by the inflow of inland rivers in Wanquan River and Tanmen Town, and the hydrodynamic process is very complicated. Therefore, it is necessary to establish a local 3D mathematical model of the artificial island and the Wanquan River.

2.2. Data Source and Model Setup

The data in this research came from the field survey data and part of the collected data were collected from the waters around Qionghai's artificial island in 2019, 2020, and 2021. The locations of the survey stations are shown in Figure 2. The pre-processing of the data and basic settings of the mathematical model are discussed below.

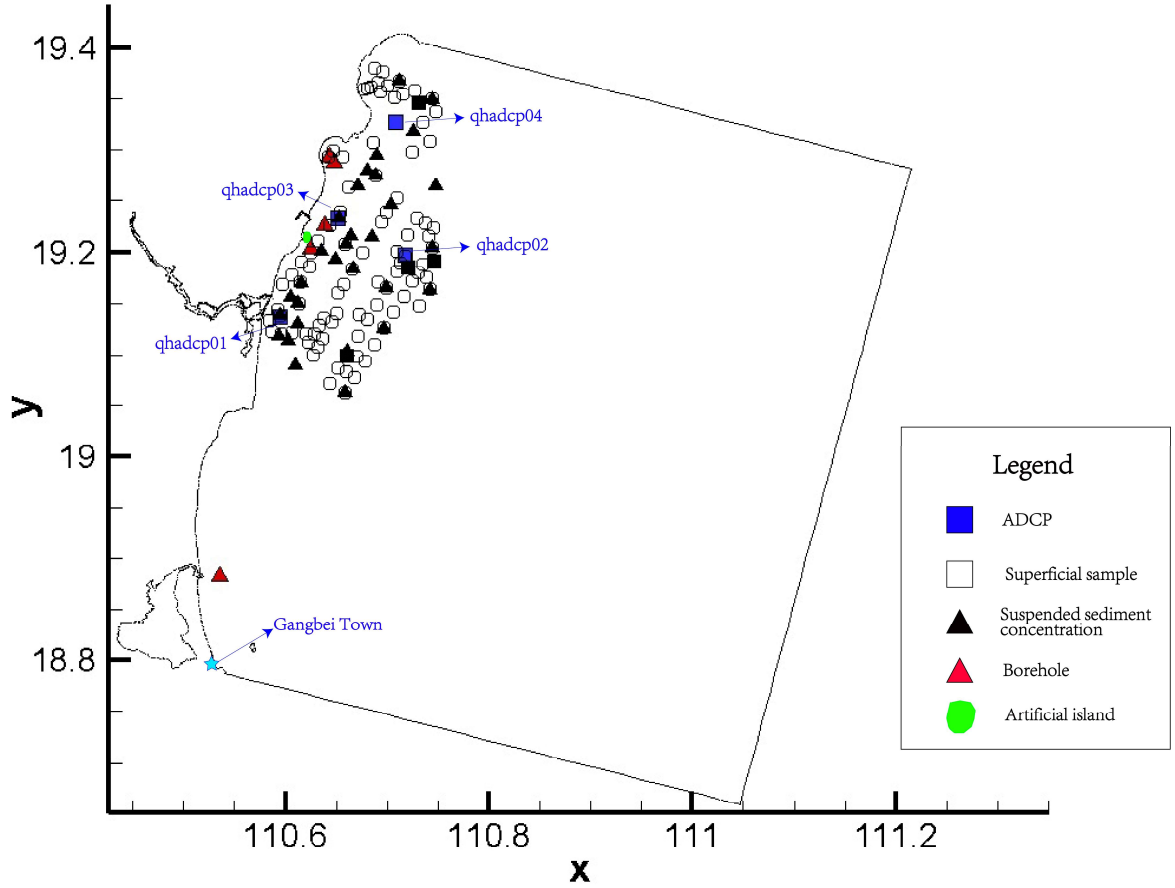

Figure 2. Field survey stations (The *x*-axis is the east longitude axis and the *y*-axis is the north latitude axis).

2.2.1. Initial Depth Condition

Based on the coastline data of Hainan Island collected by Bi Jingpeng et al. [19], we defined the calculation domain and generated a triangular unstructured grid in the study area, which was divided into 489,776 units and 249,782 nodes. The triangular grid used different lengths at the river channel, coastline, artificial island boundary line, and offshore boundary. After mesh quality optimization, the triangular mesh with uneven density was able to meet the needs of high-precision water and sediment simulation.

The topographic survey adopted a single-beam sounder to carry out an intensive survey of the marine area near the study area. The tracked line of the navigation survey is shown in Figure 3a (the *x* and *y* axes in the figure represents longitude and latitude, respectively, in decimal form of WGS1984 system, and the full text is unified). The intensive topographic survey reflects local topographic features under the influence of the artificial island, as shown in Figure 3b.

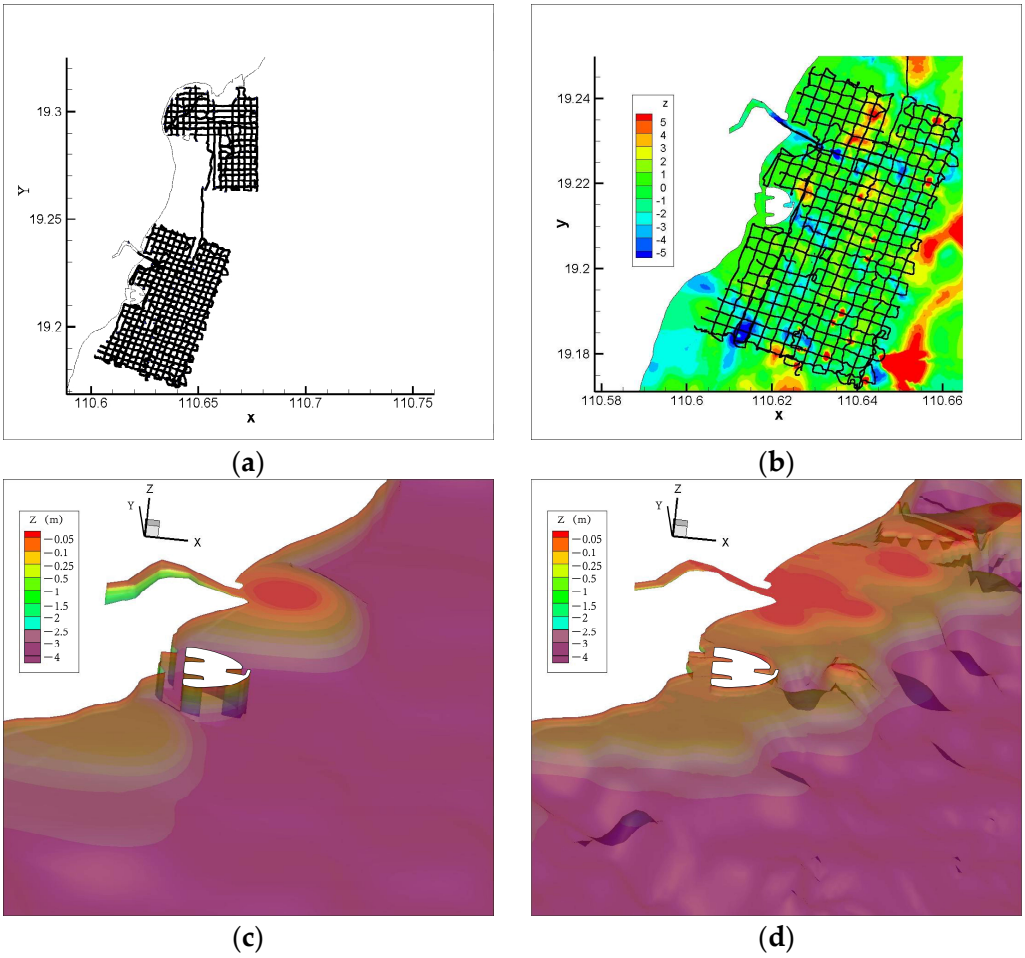

Figure 3. (**a**) Bathymetric survey line in the study area; (**b**) distribution of water depth around the artificial island; (**c**) bathymetric maps for ETOPO1 data collection; (**d**) three-dimensional topographic and geomorphic features of the study area for fusion of infill bathymetric data [The *x*-axis is the east longitude axis and the *y*-axis is the north latitude axis].

At the same time, we collected the spatial resolution of 2 km of global water depth ETOPO1 figures released by the American NOAA (https://www.ngdc.noaa.gov/mgg/global/, accessed on 15 July 2021). Due to the low spatial resolution of ETOPO1 data, which cannot accurately reflect the local topography around the artificial island (Figure 3c), the measured and collected data needed to be fused to form more accurate bathymetric data (Figure 3d) that can reflect the scour pits and silts around artificial island more clearly, in addition to more detailed siltation patterns at the mouth of Tanmen Port. Then, we interpolated the fused water depth data into the grid by using the inverse range interpolation method, which was used as the initial water depth condition for this study and laid a foundation for the numerical simulation of water and sediment in the complex near-shore environment.

2.2.2. Sediment Transport and Tidal Boundary Conditions

The open boundary included the water level boundary at the entrance of Wanquan River and the tidal driving boundary of the ocean. The 2020 daily recorded water level and suspended sediment concentration data from Jiaji Hydrographic Station at the entrance of Wanquan River were used, as shown in Figure 4. Except for flood season (concentrated from August to November), the flow and sediment transport rates of Wanquan River were very low.

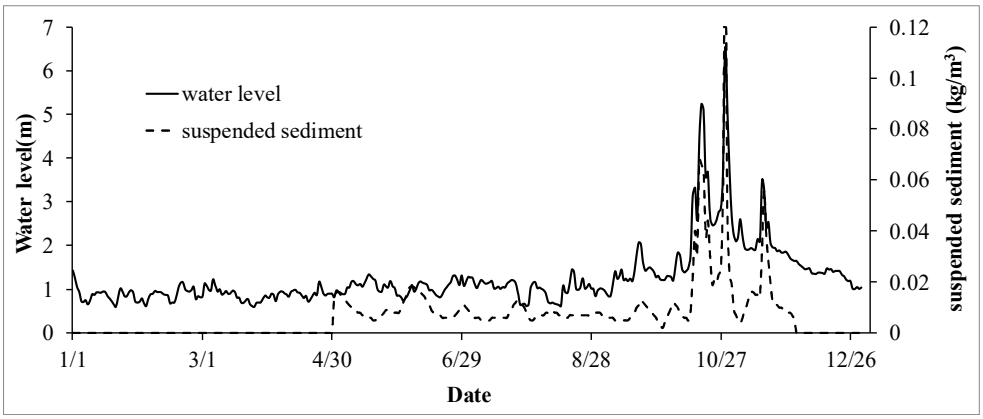

Figure 4. Changes in water level and suspended sediment concentration at the Wanquan River Jiaji Station (2020).

The tide boundary drive data from the Gangbei Tidal Station near the study area were adopted, as shown in Figure 5a. The T_TIDE program in MATLAB language was used to conduct harmonic analysis on the recorded tide data [20], and the tide value calculated by harmonic analysis was in good agreement with the measured value when applied to the ocean tidal boundary (Figure 5b).

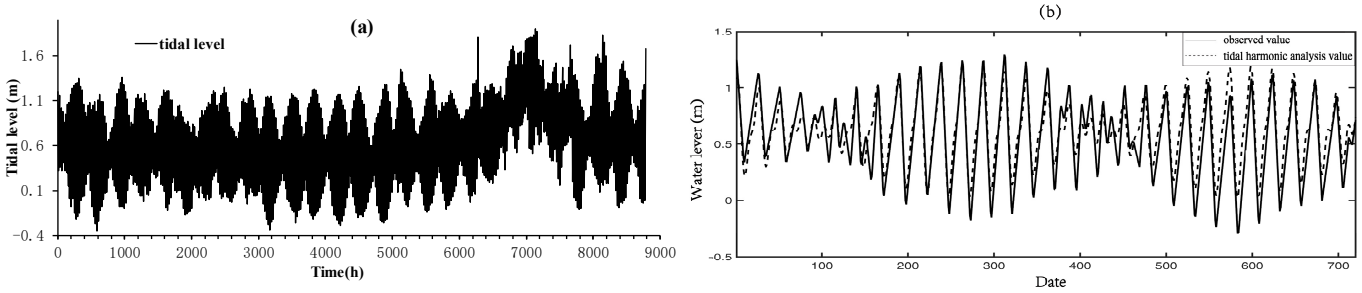

Figure 5. Tidal level and harmonic analysis recorded at Gangbei Town tidal level Station ((**a**) tidal level; (**b**) harmonic analysis).

2.2.3. Wind and Wave Conditions

The hydrodynamics and wave boundary conditions were determined using meteorological data of wind speed, wind direction, air temperature, and air pressure in 2020, which were collected from the meteorological station in Gangbei Town. In addition, for Typhoon 19 in July 2017, Gangbei Town recorded the wind field (including wind speed and direction) and water level process of the typhoon, as shown in Figure 6. The typhoon caused obvious water increases, and water increase and wind speed showed a positive correlation. At the same time, the wind direction during the typhoon was mainly northeasterly, which had a more obvious water increase effect on the Wanquan estuary and the area near Tanmen Port. Therefore, this study included both general meteorological conditions and extreme typhoon meteorological conditions, and the data were highly representative.

2.2.4. Suspended Sediment and Bed Sediment Conditions

The suspended sediment concentration affected the regional sediment movement trend and had a great influence on regional erosion and sedimentation. The data used in this study were based on the suspended sediment concentration in the middle and lower surface waters measured around the artificial island in 2020 and 2021. In addition, different types of seabed sediment also affected regional flow, suspended sand, and other indices. In this simulation, bed sand conditions were also taken into account. The data were based on bed sand and quaternary bed sand thickness surveys conducted using three shallow holes (depth < 60 cm) and 1 deep hole (about 20 m deep). Then, the suspended sediment was

divided into 5 groups according to particle size and interpolated into the calculation grid by inverse distance to form the initial distribution conditions of the suspended sediment concentration, bed sand gradation, and quaternary bed sand thickness [21].

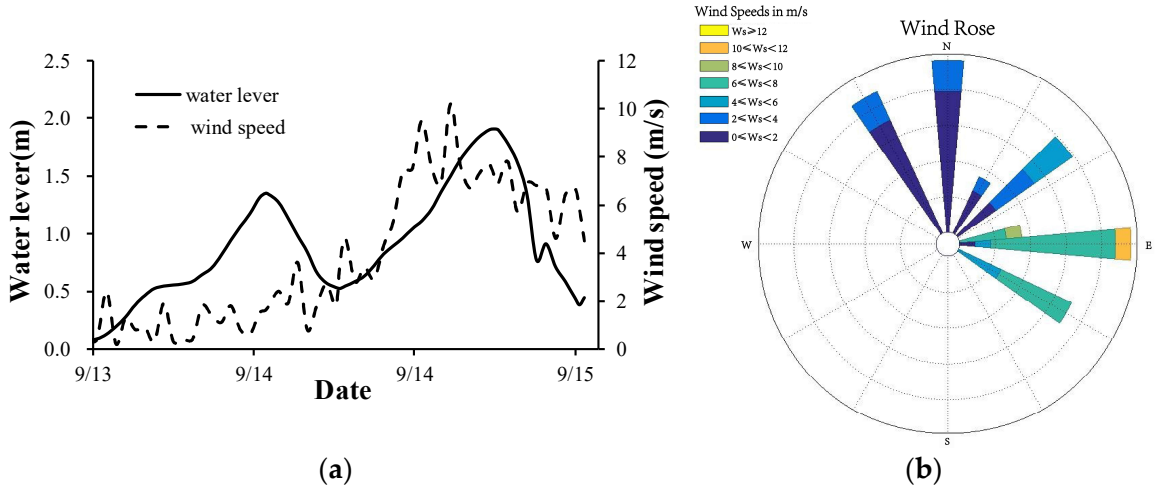

Figure 6. Water level and wind field recorded during Typhoon 19, 2017, in Gangbei Town. (**a**) Curve of typhoon water level and wind speed. (**b**) Typhoon transit wind speed rose chart.

2.3. Mathematical Model Building

In this study, SCHISM and WWM were used to simulate the water and sediment dynamics under the influence of the artificial island in the study area. Below, the mathematical model of the basic equations and modules used are introduced briefly, and the SCHISM of the specific physical principle and the numerical method can be seen at the following web site (https://geomodeling.njnu.edu.cn/modelItem, accessed on 10 August 2021).

2.3.1. Hydrodynamic Model

The hydrodynamic model adopts the SCHISM system, the full name of which is the Semi-implicit Cross-scale Hydroscience Integrated System Model, developed by the Virginia Oceanographic Institute [13]. SCHISM was widely applied in the research of many ocean engineering problems [12]. To be specific, SCHISM is not a model, but a simulation system. The core of the SCHISM simulation system is a three-dimensional hydrodynamic model based on the assumption of hydrostatic pressure, which drives other coupled modules, including a sediment model, water ecological model, water quality model, wave model, oil spill model, sea ice model, hydraulic building model, etc. The three-dimensional hydrodynamic calculation module was developed in unstructured grid mode, which was suitable for computationally complex geometric boundaries and complex terrain. The governing equations of the hydrodynamic model included a continuity equation and a momentum equation:

$$\frac{\partial u}{\partial x} + \frac{\partial v}{\partial y} + \frac{\partial w}{\partial z} = 0 \tag{1}$$

$$\frac{du}{dt} = fv - g\frac{\partial \eta}{\partial x} + K_{mh}\left(\frac{\partial^2 u}{\partial x^2} + \frac{\partial^2 u}{\partial y^2}\right) + \frac{\partial}{\partial z}\left(K_{mv}\frac{\partial u}{\partial z}\right) \tag{2}$$

$$\frac{dv}{dt} = -fu - g\frac{\partial \eta}{\partial y} + K_{mh}\left(\frac{\partial^2 v}{\partial x^2} + \frac{\partial^2 v}{\partial y^2}\right) + \frac{\partial}{\partial z}\left(K_{mv}\frac{\partial v}{\partial z}\right) \tag{3}$$

where (x, y) is the Cartesian plane coordinate (m); Z is the vertical coordinate, where upward is positive; t is the time (s); Z_{ini} is used to calculate the initial water level (m); η is the fluctuation of the free water level (m); h is the water depth (m); u, v are normal and tangential velocity (m/s); g is the acceleration of gravity (m/s^2) and is 9.81; f is the Coriolis force

coefficient (1.0487974×10^{-4}); ρ is the density of water; and K_{mh}, K_{mv} are the horizontal and vertical turbulent viscosity coefficients (m^2/s) in the flow momentum equation.

2.3.2. Wave Model

The wind-generated wave model adopts the third-generation WWM (WWM-III) model, the full name of which is the Wind Wave Model. WWM-III solves the 2D wave spectrum equation of a plane [22]. The wave spectrum equation is:

$$\frac{\partial}{\partial t}N + \nabla_X(\dot{X}N) + \frac{\partial}{\partial \sigma}(\dot{\theta}N) + \frac{\partial}{\partial \theta}(\dot{\sigma}N) = S_{tot} \tag{4}$$

where the wave motion index N is defined as:

$$N_{(t,\mathbf{X},\sigma,\theta)} = \frac{E_{(t,\mathbf{X},\sigma,\theta)}}{\sigma} \tag{5}$$

where E represents the variance density of sea level elevation; σ is the relative fluctuation frequency; and θ is the direction of fluctuation.

Wave propagation from deep water to shallow water is accompanied by complex nonlinear processes, such as bed bottom friction, wave breaking and tumbling, and wave energy input imposed by the boundary, which are considered in the source terms of Equation (4). WWM-III is transformed by Roland into a triangular unstructured grid model to achieve seamless coupling with SCHISM.

2.3.3. Sediment Model

The sediment model adopts the MORSELFE model [17], which is based on a triangular unstructured mesh and can be applied to water simulation with complex geometric boundaries and complex topography. The MORSELFE model considers the effects of waves on sediment transport and riverbed evolution. In the suspended sediment module, the transport equation was solved based on SCHISM, the Soulsby formula was used to obtain the settling rate of suspended sediment, and the bed sediment exchange model used the active bed sediment adjustment model. The bedload sediment is calculated using the Meyer–Peter–Muller formula and the Van Rijn formula.

2.3.4. Hydrodynamic Wave–Sediment Coupling Model

SCHISM, WWM-III, and the MORSELFE model all adopt an MPI parallel communication mechanism and use the same subregions and calculation grid, and so, there is no need to perform interpolation calculations. Compared to the use of couplers to perform interpolation conversion between grids of different types and resolutions, the hard-coded coupling mode in this study avoided the problem of interpolation error. Because SCHISM, WWM-III, and the MORSELFE model used different discrete time formats, different computing time steps were adopted, and the information exchange of the models was performed at a certain frequency set by the user. As shown in Figure 7, during information exchange, water level (Zl), seabed topography (Zb), wet and dry terrain markers and velocity (U, V) of SCHISM and some meteorological driving data, including wind speed (Uwind, Vwind) and air pressure, are transferred to WWM-III. The wave direction (Dw), wave height (Hw), wave length (Lw), and wave period (Pw) of WWM-III were transferred to SCHISM. Radiation stress (Rs), energy dissipation (Es), and orbital wave velocity (So) calculated by WWM-III were unidirectionally transferred to the MORSELFE model, while the suspended sediment concentration (SS) and velocity (U, V) calculated by SCHISM were unidirectionally transferred to the MORSELFE model. The above variable exchange was completed in memory, and the efficient communication mechanism based on the MPI library realized the variable exchange on different processes.

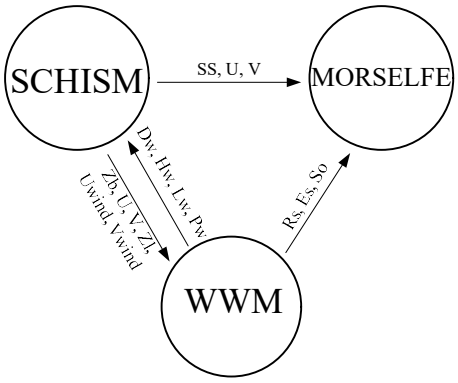

Figure 7. Framework of the hydrodynamic wave–sediment coupling simulation system.

3. Results

Model verification was required to complete a model's construction. The verified data measured were the water velocity, wave parameters (including significant wave height and wave period), and suspended sediment concentration at four stations. The four measuring points are shown in Figure 2, among which the two stations in the nearshore area, qwadcp01 and qwadcp03, were close to the artificial island. In addition, two sites, qwadcp02 and qwadcp04, were located in deep water. Based on the settings of the mathematical model above, the simulation period of 1 year was run, but only about 2 days of continuous synchronous observation data were used to verify the numerical simulation results of wind and wave flow. The accuracy of the model was verified using short-term measured data, and the influence of the artificial island on the topographic evolution of the coastal region was determined via long-term numerical simulation.

3.1. Velocity Verification

As shown in Figure 8a,b, the vertical velocity basically conformed to the decreasing law of the velocity of water facing the seabed. The velocity of water near the sea surface generally reached about 0.30 m/s, while the velocity of qwadcp01 and qwadcp03 stations in the offshore area decreased significantly and decreased to 0.02 m/s at the depth of 20 m. However, the vertical velocity distribution pattern of qwadcp02 and qwadcp04 sites in deep water was more complex. From 0 to 10 m, the velocity varied in the range of 0.2 to 0.3 m/s, while from 10 m depth below, the velocity gradually decreased to about 0.1 m/s, and the velocity was more uniform in the range of 20 to 40 m depth. Keep it at about 0.1 m/s. In general, the calculated flow velocity was in good agreement with the measured flow velocity. The accurate simulation of hydrodynamic conditions laid a foundation for the simulation of sediment transport and topographic evolution.

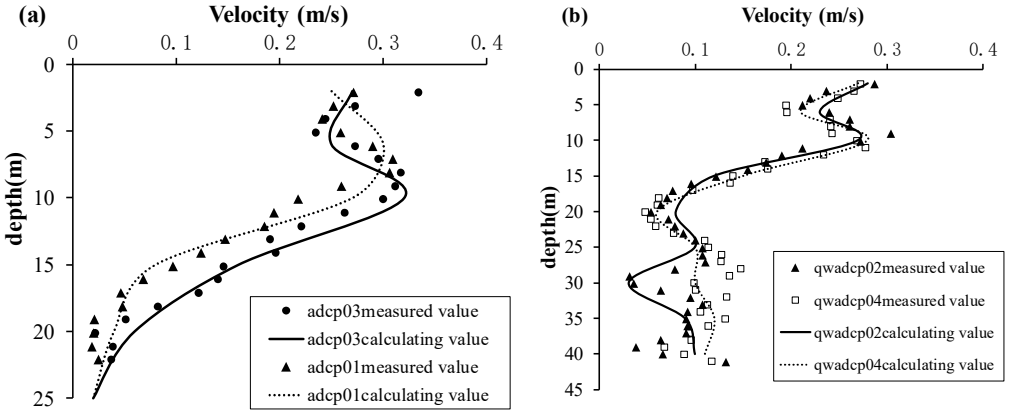

Figure 8. ADCP velocity verification ((**a**) qwadcp 01 and qwadcp 03 measurement points; (**b**) qwadcp 02 and qwadcp 04 measuring points).

3.2. Wave Simulation Verification

The significant wave height Hs (m) and wave period Tp (s) measured at the four measuring points in Figure 2 were used to verify the calculation accuracy of WWM-III. As shown in Figure 9a, the significant wave height of the qwadcp02 measuring point far from the coast reached 2.5 m, and the unsteady process was more obvious. At the qwadcp01 measuring point near the mouth of the Wanquan River in Figure 9b, the significant wave height of wind waves reached the maximum value of 1.2 m at 12 h, because it was affected by the runoff of the Wanquan River. The runoff of Wanquan River was opposite to the higher tidal current of open sea and cancelled each other out, making the wave height smaller than that of open sea area, which reflected the spatial difference of wind waves. The wave periods in Figure 9c,d show that the difference in the wave periods between these two measuring points was not significant, and both varied between 6 and 18 s. In general, the calculated results of WWM-III were in good agreement with the measured data and, thus, reflected the wave characteristics around the artificial island.

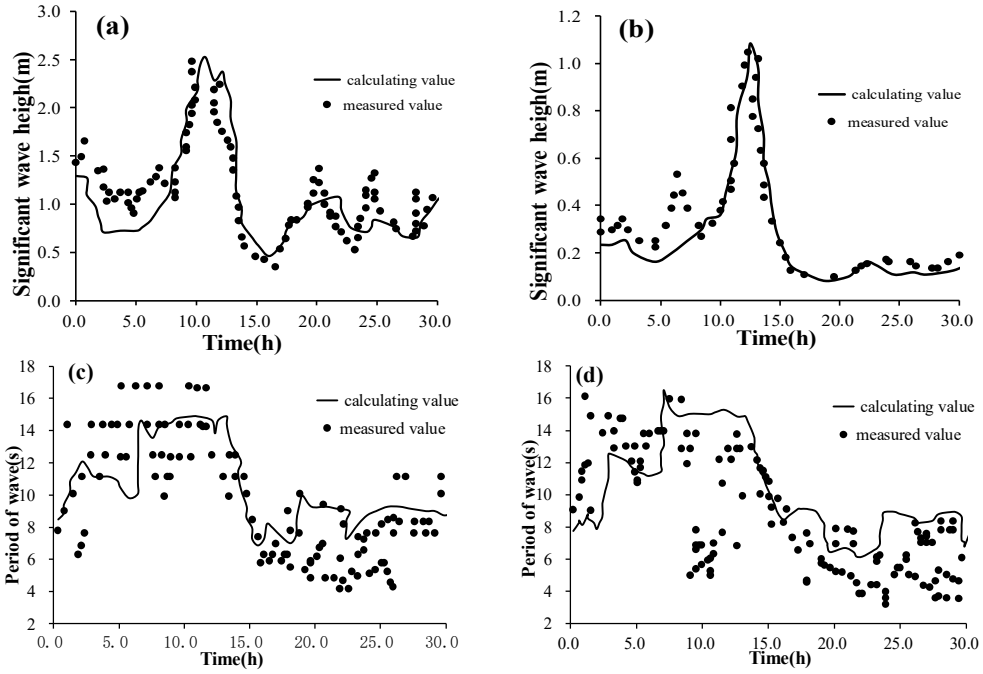

Figure 9. Verification of significant wave height and wave period ((**a**) significant wave height at qwadcp02; (**b**) significant wave height at qwadcp01; (**c**) wave period at qwadcp02; (**d**) wave period at qwadcp01).

3.3. Verification of Suspended Sediment Concentration

Due to the limitations of offshore real-time observation operation conditions, the effective time series values of the suspended sediment concentration were only obtained at qwadcp02, but the instantaneous values of suspended sediment concentration were obtained from 13 points around the artificial island and the waters near the mouth of the Wanquan River. These values were used as the initial distribution conditions of the suspended sediment concentration via spatial interpolation into the calculation grid, as shown in Figure 10a. The surface suspended sediment concentration over Tanmen Harbor formed two high concentration zones (about 0.15 kg/m^3) and one low concentration zone (sediment concentration <0.01 kg/m^3); the concentration at the entrance of Tanmen Port was very low, and a high sediment content area was formed in the offshore area (sediment concentration >0.35 kg/m^3). The formation of areas with high sediment concentrations was related to human activities near the artificial island and fishing ports. The measured suspended sediment concentration at qwadcp02 showed no significant rule, but it was

roughly consistent with the variation trend of the calculated value, as shown in Figure 10b, which showed a decreasing trend during the simulation period.

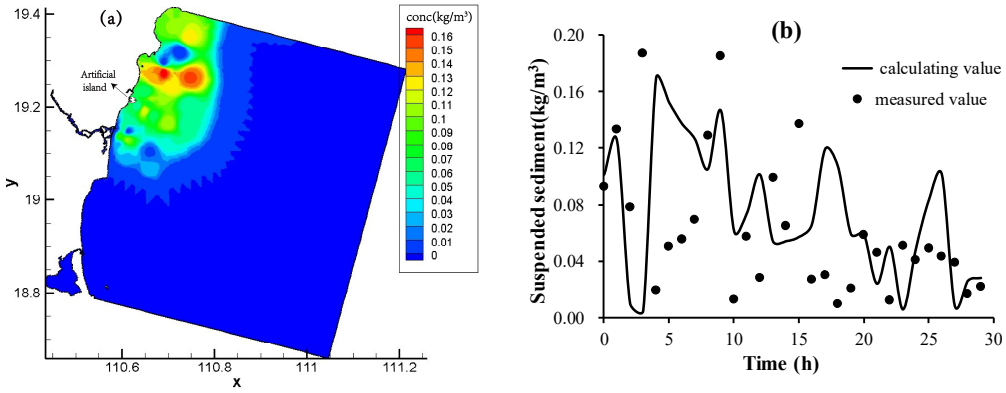

Figure 10. (**a**) Distribution of suspended sediment concentration [the *x*-axis is the east longitude axis and the *y*-axis is the north latitude axis]; (**b**) suspension sediment simulation validation.

4. Discussion

Based on the verified coupled model driven by measured water and sediment data presented above, the evolution of the near-shore topography under the disturbance of the artificial island and its causes were analyzed, and the trend of the topographic evolution after the removal of the artificial island is discussed.

The existence of the artificial island will interfere with the local flow field, causing the formation and shedding of vortices. Different hydrodynamic characteristics were shown during the different advances and retreats of the tides relative to the coastline, as shown in Figure 11a. In the tidal surge stage, an obvious beam flow area was formed between the artificial island and the coastline, and a vortex area was formed behind the island. In addition, there was a dry terrain area near Tanmen Port, and the dry and wet terrains changed with the change in the tidal current, which also shows the superiority of SCHISM's dry and wet terrain processing algorithm. In the stage of an abrupt tidal current (Figure 11b), the channel runoff from Tanmen Harbor was large, forming a significant coastal current from bottom to top (from west to east), constantly transporting the sediment from the Wanquan River. Meanwhile, the seabed around the artificial island was mainly composed of sand and silt, which were non-cohesive and easy to stir up, contributing to the sediment accumulation between the artificial island and the coastline. With the passage of time, the tombolo bar was gradually formed. In general, multi-directional currents and sediment transport from the artificial island and shoreline-confined areas, channel runoff and coastal currents, and ocean-directed tidal currents contributed to the local seabed topography of the artificial island.

In order to further simulate the influence of the artificial island on regional changes in scour and siltation, we simulated an ideal scenario of the complete removal of the artificial island. The simulation compared the distribution of topographic scour and siltation thickness around the artificial island one year after its removal and combined the results with the actual situation of active beds of the seabed surveyed by drilling, that is, the thickness of the quaternary was generally less than 2 m. The results show that in the case of the artificial island, as shown in Figure 12a, about 0.1 m of siltation occurred between the island and shoreline and on both sides of the island, with a −0.1 m scour thickness behind it. After the removal of the artificial island, as shown in Figure 12b, the erosion and siltation on both sides of and behind the island decreased (the thickness was less than 0.05 m) and tended to return to the natural bed morphology. However, the siltation morphology remained at the local location of the shore at 0.1 m.

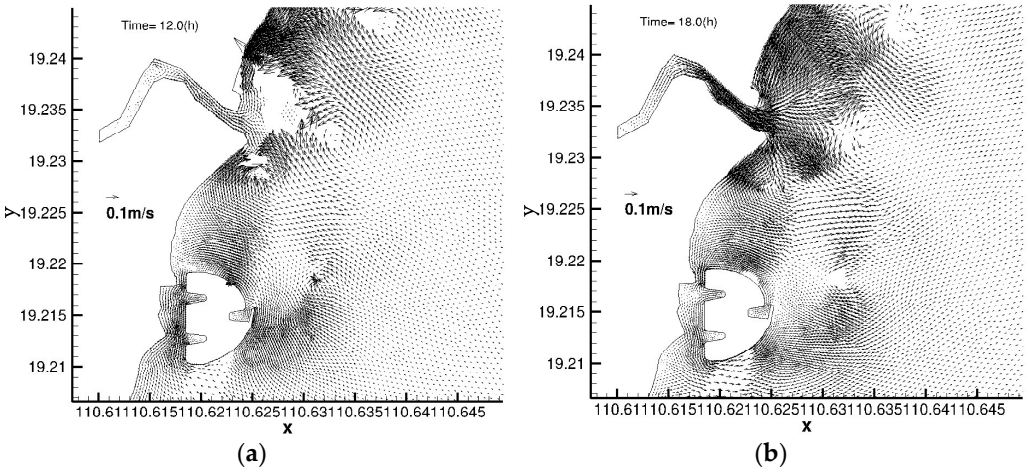

Figure 11. Vector diagram of velocity around the artificial island ((**a**) surge tidal current field; (**b**) plunging tidal current field) [the *x*-axis is the east longitude axis and the *y*-axis is the north latitude axis].

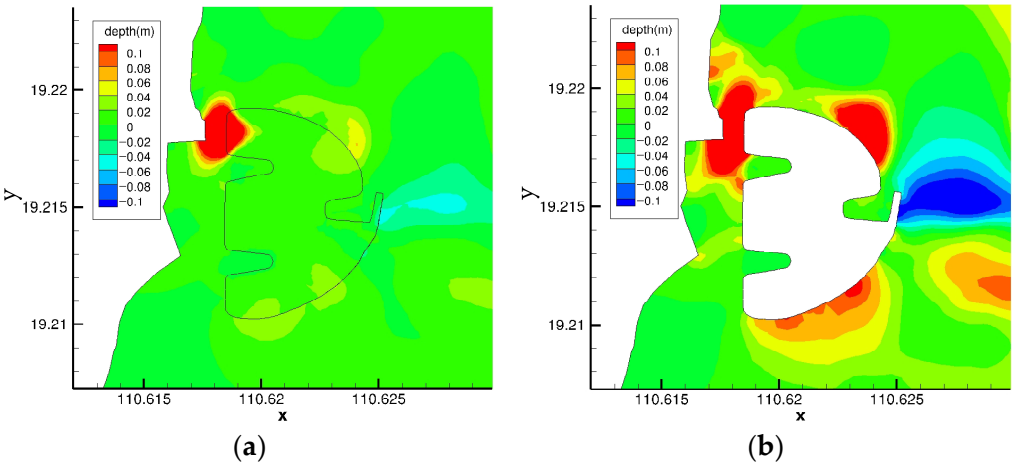

Figure 12. Impact assessment of the artificial island's demolition ((**a**) thickness distribution of scour and silt around the artificial island after demolition; (**b**) distribution of scour and silt thickness around the artificial island under standard conditions [the *x*-axis is the east longitude axis and the *y*-axis is the north latitude axis].

A comprehensive analysis of the sediment transport and topographic evolution mechanism around the artificial island concluded that when the artificial island exists, a beam will form between the artificial island and the coastline, which will meet the coastal current coming to Tanmen Port (see Figure 11), resulting in the siltation between the artificial island and the coast. An eddy wake was formed on the back surface of the artificial island, which interacted with the tidal current and formed scour pits on the back surface (see Figure 3b). After the complete removal of the artificial island, the sea bed developed towards a balance of erosion and silt. In conclusion, due to the synthetic effect of the beam and the water-retaining effect on the man-made island, the coastal current and the tidal current led to the artificial island having a complex influence on the water and sediment transport and topographic evolution.

5. Conclusions

In this study, a coupled simulation system based on an unstructured grid SCHISM, the WWM-III wave model, and the MORSELFE sediment transport and topographic evolution model was used to simulate the dynamic processes of local water and sediment transport and the topographic evolution under interference from an artificial island in the offshore

area of Qionghai, Hainan Province. The field-measured data can drive complex coupled simulations of the wind, waves, and sediment transport. In particular, the local small-scale geometric characteristics of the artificial island significantly affect the distribution of hydrodynamics, suspended sediment, and topographic evolution in local waters. The coupled hydrodynamic wave–sediment simulation system based on a unified unstructured grid can reflect detailed information of the cross-scale, near-shore environmental evolution.

Local disturbance from the artificial island led to the formation of eddies in the surrounding waters during the ebb and flow of the tides, resulting in the formation of local siltation and erosion pits, especially near the angle between the island and the coastline. Over time, siltation will form into tombolo bars, and erosion will be caused behind local walls such as the sharp corners of the artificial island. The simulation results showed that after the removal of the artificial island, most of the thickness of the scouring and silting will be reduced, and the seabed can return to its natural equilibrium state; however, the silting caused by local coastline morphology will still exist.

There were also shortcomings in this study, such as the insufficient observational data on suspended sediment concentration and topographic evolution, which limited the demonstration and disclosure of more detailed information about near-shore sediment transport and topographic evolution under interference from the artificial island. Due to the lack of observational data on hydrodynamics, sediment transport, and topographic evolution during typhoons, the topographic evolution during typhoons was not analyzed in this paper. The influence of individual extreme typhoon events on the evolution of the coastal environment combined with the influence of the artificial island also needs to be studied in the future.

Author Contributions: Thanks to all the authors for their joint efforts, which were as follows. Investigation, K.Y., M.F., H.W. and G.F.; writing—original draft preparation, G.F.; writing—review and editing, J.L., K.Y., Y.S. and X.W.; project administration, J.L. All authors have read and agreed to the published version of the manuscript.

Funding: This research was funded by Science and Technology Innovation Fund of Command Center of Integrated Natural Resources Survey Center (KC20220009) and funded by the Comprehensive Survey of Natural Resources in HaiChengWen Coastal Zone, grant number DD20230414.

Institutional Review Board Statement: Not applicable.

Informed Consent Statement: Not applicable.

Data Availability Statement: The data are unavailable due to privacy.

Acknowledgments: Thanks to Li Jian for his guidance and help. I would like to thank all the authors for writing this article together. Finally, I would like to express my sincere thanks to the editors and reviewers for their comments and suggestions.

Conflicts of Interest: The authors declare no conflict of interest.

References

1. Yan, K. *Coastal Engineering*; Ocean Press: Beijing, China, 2002; pp. 120–130.
2. Peng, B.; Hong, H.; Chen, W.; Xue, X.; Cao, X.; Peng, J. Ecological Damage Appr aisal of Sea Reclamation: Theory8 Method and Application. *J. Nat. Resour.* **2005**, *5*, 714–726.
3. Zhu, G.; Xu, X. Research review on environmental effects of land reclamation from sea. *Ecol. Environ. Sci.* **2011**, *20*, 761–766.
4. Yang, Y.; Liu, X.; Qiu, R.; Yang, W. The analysis of shoreline changes respond to artificial island project of Dongjiao coco forest based on DSAS and SMC. *Period. Ocean. Univ. China* **2017**, *47*, 162–168.
5. Li, S. Study on the influence of artificial island on dynamic sediment environment and beach erosion and deposition evolution of sandy coast. *Ocean. Eng.* **2021**, *39*, 144–153.
6. JETRO. *Feasibility Study of the Construction of an Artificial Island at the Pacific Entrance to the Panama Canal*; Belgian Press: Brussels, Belgium, 2004.
7. Salahuddin, B. The Marine Environmental Impacts of Artificial Island Construction. *J. Environ. Manag.* **2006**, P15.
8. Gong, W.P.; Li, C.Y.; Lin, G.Y.; Mo, W.Y. Application of DELFT 3D model for plan design of an artificial island—A case study for the artificial island construction in The Riyue Bay, Wanning City, Hainan Island. *Ocean Eng.* **2012**, *30*, 35–44.

9. Tan, X.; Gao, J. Impact of the Sanya new airport artifial islands project on tidal dynamics of the Hongtang Bay. *Mar. Sci. Bull.* **2019**, *21*, 1–15.
10. Kuang, C.; Jiang, L.; Ma, Y.; Qiu, R. Wave-current coupled hydrodynamic responses to artifical island and beach nourishment projects. *J. Tongji Univ.* **2019**, *47*, 38–46.
11. Yang, F.; Pan, J.; Wang, H. Study on the design wave on the artificial island of Hong Kong-Zhuhai-Macao Bridge while considering the extreme weather I: Selection method of the typhoon track in numerical wave simulation. *Adv. Water Sci.* **2019**, *30*, 892–901.
12. Warner, J.C.; Sherwood, C.R.; Signell, R.P.; Harris, C.K.; Arango, H.G. Development of a three-dimensional, regional, coupled wave, current, and sediment-transport model. *Comput. Geosci.* **2008**, *34*, 1284–1306. [CrossRef]
13. Zhang, Y.; Baptista, A.M. SCHISM: A semi-implicit Eulerian-Lagrangian finite-element model for cross-scale ocean circulation. *Ocean Model.* **2008**, *21*, 71–96. [CrossRef]
14. Zhang, Y.; Ye, F.; Stanev, E.V.; Grashorn, S. Seamless cross-scale modeling with SCHISM. *Ocean Model.* **2016**, *102*, 64–81. [CrossRef]
15. Roland, A. Development of WWM II: Spectral Wave Modeling on Unstructured Meshes. Ph.D. Thesis, Technische Universität Darmstadt, Darmstadt, Germany, 2009; pp. 25–38.
16. Roland, A.; Zhang, Y.J.; Wang, H.V.; Meng, Y.; Teng, Y.-C.; Maderich, V.; Brovchenko, I.; Dutour-Sikiric, M.; Zanke, U. A fully coupled 3D wave-current interaction model on unstructured grids. *J. Geophys. Res. Oceans* **2012**, *117*, C00J33. [CrossRef]
17. Pinto, L.; Fortunato, A.B.; Zhang, Y.; Oliveira, A.; Sancho, F.E.P. Development and validation of a three-dimensional morphodynamic modelling system. *Ocean. Model.* **2012**, *57–58*, 1–14. [CrossRef]
18. Fu, G.; Song, Y.; Yuan, K. A study on the erosion and siltation evolution of the neighboring coast caused by the enclosure of Boao Coral island. *Mar. Environ. Sci.* **2022**, *41*, 174–179.
19. Bi, J.; Zhang, L.; Song, Q.; Sui, Y.; Wen, L. Coastline Dataset of Hainan Island during 1987–2017. [DB]. V1. Science Data Bank: 2019. Available online: https://www.scidb.cn/en/detail?dataSetId=633694461133586432 (accessed on 25 April 2023).
20. Pawlowicz, R.; Beardsley, B.; Lentz, S. Classical tidal harmonic analysis including error estimates in MATLAB using T_TIDE. *Comput. Geosci.* **2002**, *28*, 929–937. [CrossRef]
21. Song, Y.W.; Yuan, K.; Fu, G.W. *Report for the Geological and Coastal Surveying Project of Qionghai-Wanning in Hainan Province (No. DD20208012)*; Haikou Marine Geological Surveying Center affiliated with China Geological Survey Bureau: Beijing, China, 2021.
22. Clodman, S. A Generalized Parametric Wind Wave Model. *J. Great Lakes Res.* **1994**, *20*, 613–624. [CrossRef]